



ORIGINAL ARTICLE

Investigating heat transfer and fluid flow betwixt parallel surfaces under the influence of hybrid nanofluid suction and injection with numerical analytical technique



Seyyed Amirreza Abdollahi ^{a,*}, As'ad Alizadeh ^b, ilia Chiniforooshan Esfahani ^c,
Meysam Zarinfar ^{d,*}, Pooya Pasha ^e

^a Mechanical Engineering, Energy conversion, Faculty of Mechanical Engineering, Tabriz University, Tabriz, Iran

^b Department of Civil Engineering, College of Engineering, Cihan University-Erbil, Erbil, Iraq

^c College of Engineering, Northeastern University, Boston, MA, 02115, United States

^d Department of Civil engineering, Faculty of Bu-Ali Sina university, Hamedan, Iran

^e Department of mechanical Engineering, Mazandaran university of science and technology, Babol, Iran

Received 24 October 2022; revised 30 January 2023; accepted 24 February 2023
Available online 8 March 2023

KEYWORDS

Numerical Method;
Radial Basis Function
(RBF);
Hybrid nanofluid;
Nusselt number;
Reynolds number;
Rotating system;
Schmidt number

Abstract In this article, by using a novel approach, the heat transfer related to the hybrid nanofluid flow containing graphene oxide and copper particles in pure water, which is located in a rotating system, is analyzed. The innovation of this article, using a new approach, explores the heat transfer related to the flow of mixed nanofluid containing graphene oxide and copper particles in pure water, which is in a rotating system, and using the RBF method for the first time Investigates differential equations and simplified coupled equations. The radial basis function methodology was utilized to solve the equations, and the outcomes were compared to those obtained using the Runge–Kutta–Fehlberg numerical method. In this problem, there are much necessary quantities such as the Reynolds number, Nusselt number, Schmidt number, Thermophoretic quantity, Brownian quantity, Injection quantity, and Rotation quantity so that communication between them is investigated. Based on the results, with the increase of Reynolds number, the amount of heat transfer decreases significantly, and with the decrease of heat flows from the surfaces, the flow rate of fluid and nanofluid decreases. However, the concentration of nanomaterials reaches a maximum value as the Reynolds number increases.

© 2023 THE AUTHORS. Published by Elsevier BV on behalf of Faculty of Engineering, Alexandria University. This is an open access article under the CC BY-NC-ND license (<http://creativecommons.org/licenses/by-nc-nd/4.0/>).

* Corresponding authors.

E-mail addresses: asgarimohammad11@yahoo.com (S.A. Abdollahi), zarinfar@basu.ac.ir (M. Zarinfar).

Peer review under responsibility of Faculty of Engineering, Alexandria University.

<https://doi.org/10.1016/j.aej.2023.02.040>

1110-0168 © 2023 THE AUTHORS. Published by Elsevier BV on behalf of Faculty of Engineering, Alexandria University. This is an open access article under the CC BY-NC-ND license (<http://creativecommons.org/licenses/by-nc-nd/4.0/>).

Nomenclature

C	Concentration of hybrid nanofluid
C_f, \tilde{C}_f	Skin friction coefficients
C_p	Specific heat capacity at constant pressure ($J.kg^{-1}.K^{-1}$)
\mathcal{D}_B	Diffusion coefficient of the diffusing species
P^*	Modified fluid pressure (Pa)
h	Distance between the plates (m)
k	Thermal conductivity ($W.m^{-1}.K^{-1}$)
K_r	Rotation quantity
L	Length of the plate (m)
\mathcal{N}_b	Brownian motion quantity
\mathcal{N}_t	Thermophoretic quantity
Pr	Prandtl numeral
Nu	Nusselt numeral
Sc	Schmidt numeral
\mathcal{R}	Reynolds numeral
T	Temperature (K)
s	Shape factor
u, v, w	Velocity components along x, y, z axes respectively ($m.s^{-1}$)

Abbreviation

PDE	Partial Differential Equation
ODE	Ordinary Differential Equation
AGM	Akbari – Ganji's Method
ADM	Adomain Method
HAM	Homotopy Analysis Method

DTM	Differential Transform Method
RBF	Radial Basis Function
FEM	Finite Element Method
RKF	Runge – Kutta – Fehlberg
MHD	Magnetohydrodynamic
MWCNT	Multi – Walled Carbon Nanotube

Greek symbols

ρ	Density of fluid ($kg.m^{-3}$)
θ	Dimensionless temperature
μ	Dynamic viscosity ($kg.m^{-1}.s^{-1}$)
ϕ	Dimensionless concentration
α	Thermal diffusivity
η	Dimensionless variable
ϑ	Kinematic viscosity ($m^2.s$)
λ	Dimensionless suction/injection quantity
Ω	Constant rotation velocity

Subscripts

s	Solid particles
h	Hot
o	Cold
bf	Base fluid
nf	Nanofluid
hnf	Hybrid nanofluid

1. Introduction

Investigating heat transfer and fluid flow between surfaces has become a subject of interest among researchers in the past years, due to the apparent diversity of its technological and capable applications. The rotating flow of nanofluids is one of the typical problems with critical utilization in engineering, industry, and technology. In particular, studying nanofluids between parallel plates vhas essential applications in accelerators, MHD generators, and pumps. Extrusion, wire drawing, glass fiber manufacturing, melt-spinning, hot rolling, and other technical operations, for instance, can all benefit from it. As a result, extensive research has been conducted to examine the heat and stream exchange properties between two pages. Chamkha et al. [1] proved that the Duan-Rach accost is a valid method to discover a systematic solution without the need to employ a numerical approach for computing any unclear quantity s by using it in their study of magneto-hydrodynamic flow through two equal rotating sheets. Hus-sain et al. [2] investigated the combined impressions of rotation and Hall outflow on an unsteady magneto-hydrodynamic free-convective heat and mass transfer flow of an incompressible, viscous and electrically conducting fluid past a permeable body, taking ramped temperature and surface concentration into account. The indeterminate flow and heat transfer development of an unsteady flow caused by a single, rotating, the vertically moving disc was looked into by Turkyilmazoglu [3] it was concluded that the vertical movement of the disc can have a remarkable influence on different conjugations, includ-

ing drag, and heat transfer. In another work [4], he analyzed the flow behavior and two- deduction heat transfer rate of suspended specks with the fluid over a pivoting disk. Zahir et al. [5] examined the case of a third-grade non-Newtonian nanofluid in a rotating system, flowing through two parallel plates in a three-dimensional coordinate set, both Brownian motion and thermophoresis effect taken into consideration. He characterized the influence of different values of variant quantities on velocity, temperature, heat and mass flux, while successfully showing the isotropy of the Homotopy analysis style per an alteration of the physical quantity. Zahir et al. [6] solved the problem of micropolar nanoparticle effluvium of Casson effluvium under the Hall current effect and thermal radiation between two rotating parallel plates. The nanofluid bioconvection under temperature-dependent viscosity and thermal conductivity was solved numerically by Xun et al. [7] in a three-dimensional rotating system, with the aid of Matlab bvp4c ODE solver. It was found that the viscosity variation quantity affects the Sherwood number and the local skin friction coefficient, In contrast, the thermal conductivity variation quantity plays a more prominent role in the wall motile microorganisms' flux and positional Nusselt number changes. Later, A new model was introduced by Pourmehran et al. [8] to examine a laminar nanofluid's flow between two contracting rotating plates in more detail, Brownian motion and Patel model included. The results indicated that Silver had the highest heat transfer rate used as the nanoparticle. Yin et al. [9] investigated three different nanofluids outflow within the outspread course over a pivoting disk under the assumption of a uniform

stretching rate. He concluded that many characteristics are a function of the stretching strength. Abro et al. [10] proved the higher efficiency of solar collectors in absorbing incoming sunlight by modeling MHD turning Jeffery nanofluid stream of Graphene-based SWCNTs and MWCNTs made stable in a proliferous medium, by employing Caputo–Fabrizio fractional equations in their analytical proposed solution. Also, studies about the dimensionless equations of equations with partial derivatives for the flow of different nanomaterial's under the shadow of Lorentz force and magnetic parameters around the curves and rotating plates by researchers named Kardi and Jawad and their colleagues [11–16] took place in recent years. Hayat et al. [17] studied the case of magneto-hydrodynamic peristaltic flow of Al_2O_3 and CuO nanoparticles in a rotating frame under thermal radiation, using a lubrication approach. They noted that the entropy era could be a work of radiance, and temperature enhances when internal heat generation increases but falls when the radiation increases. Shah et al. [18] have explored the MHD three-dimensional Jeffery nanofluid through parallel plates beneath the impact of the Lobby stream. By assuming one of the plates to be stretching and the other, fixed in modeling the system, HAM could be employed in analytically solving the problem and the physical quantity s could be discussed. In another study, Shah et al. [19] solved the case of a micropolar nanoparticle betwixt two equal turning plates under the Hall stream and an electric field's effect analytically, using HAM.

Much research has been done on the heat and mass transfer mechanisms of effluents, as discussed in the literature. betwixt two equal lateral surfaces where both the fluid and the sheets were rotating, However, the RBF technique, which is a remarkably accurate method for testing velocity, temperature, and concentration bins, has not been utilized quite often [20–25]. Saeed Dinarund and his colleagues [26–33] have registered many studies and research in the field of thermophysical properties of nanofluids and the effects of Brownian force fluid parameters and thermophoretic parameters, and most of these studies have been conducted around porous plates and rotating disks. Bhattad and Biswas and their colleagues [34–50] did a parcel of investigation within the field of on hybrid nanofluid flow and effects of the magnetic parameter around plate converters, and porous systems while calculating the amount of thermal radiation and Nusselt number with numerical and analytical, finite element and finite volume methods. The central reason for this investigation to apply the radial basis function (RBF) technique to dissolve the nonlinear differential conditions of mass and heat transfer in a pivoting framework with an extending sheet. On the profiles of concentration, velocity, and temperature, the effects of essential and influential quantities including Reynolds numerical, Nusselt number, Schmidt number, rotation, injection, and Thermophoretic and Brownian quantities are illustrated. Finally, the influence of the nanoparticle form factor on the profile and the influence of hybrid nanoparticles were demonstrated. It should be

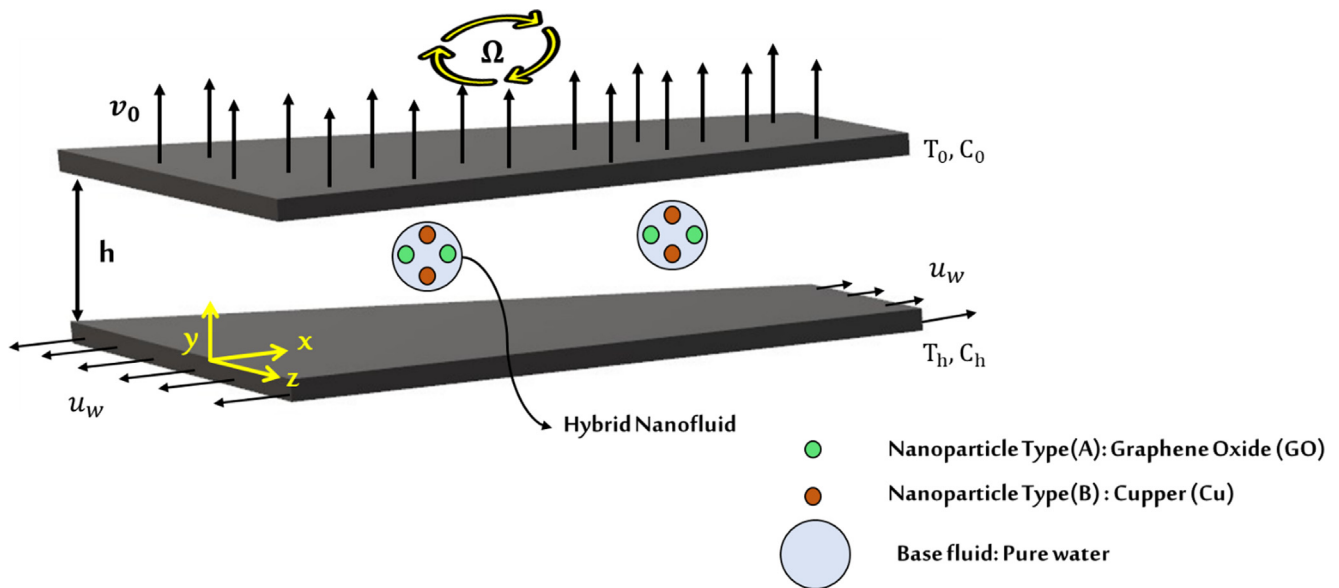


Fig. 1 Geometry of the problem.

Table 1 Thermo-physical attributes of base liquid and nanoparticles.

Physical properties	$\beta \times 10^5 (1/K)$	$k (W/mK)$	$C_p (J/kgK)$	$\rho (kg/m^3)$
Graphene Oxide (GO)	58	5000	717	1800
Copper (Cu)	44	401	385	8933
Pure water	1.89	0.613	4179	997.1

Table 2 Thermo-physical attributes model of hybrid nanofluid [11–12–13].

Properties	Nanofluid	Hybridnanofluid
Density	$\rho_{nf} = (1 - \phi)\rho_f + \phi\rho_s$	$\rho_{hnf} = (1 - \phi_2)[(1 - \phi_1)\rho_f + \phi_1\rho_{s1}] + \phi_2\rho_{s2}$
Dynamic Viscosity	$\mu_{nf} = \frac{\mu_f}{(1 - \phi)^{2.5}}$	$\mu_{hnf} = \frac{\mu_f}{(1 - \phi_1)^{2.5}(1 - \phi_2)^{2.5}}$
Coefficient of thermal expansion	$(\rho\beta)_{nf} = \phi(\rho\beta)_s + (1 - \phi)(\rho\beta)_f$	$(\rho\beta)_{hnf} = (1 - \phi_2)[(1 - \phi_1)(\rho\beta)_f + \phi_1(\rho\beta)_{s1}] + \phi_2(\rho\beta)_{s2}$
Electrical conductivity	$\frac{\sigma_{nf}}{\sigma_f} = 1 + \frac{3(\sigma - 1)\phi}{(\sigma + 2) - (\sigma - 1)\phi}$	$\sigma_{hnf} = \sigma_{bf} \left[\frac{\sigma_{s2} + 2\sigma_{bf} - 2\phi_2(\sigma_{bf} - \sigma_{s2})}{\sigma_{s2} + 2\sigma_{bf} + \phi_2(\sigma_{bf} - \sigma_{s2})} \right]$ where $\sigma_{bf} = \sigma_f \left[\frac{\sigma_{s1} + 2\sigma_f - 2\phi_1(\sigma_f - \sigma_{s1})}{\sigma_{s1} + 2\sigma_f + \phi_1(\sigma_f - \sigma_{s1})} \right]$
Heat capacity	$(\rho C_p)_{nf} = (1 - \phi)(\rho C_p)_f + \phi(\rho C_p)_s$	$(\rho C_p)_{hnf} = (1 - \phi_2)[(1 - \phi_1)(\rho C_p)_f + \phi_1(\rho C_p)_{s1}] + \phi_2(\rho C_p)_{s2}$
Thermal conductivity	$\frac{k_{nf}}{k_f} = \frac{((s-1)k_f + k_s) + (s-1)\phi(k_s - k_f)}{(s-1)k_f + k_s - \phi(k_s - k_f)}$	$k_{hnf} = k_{bf} \left[\frac{k_{s2} + (s-1)k_{bf} - (s-1)\phi_2(k_{bf} - k_{s2})}{k_{s2} + (s-1)k_{bf} + \phi_2(k_{bf} - k_{s2})} \right]$ where $k_{bf} = k_f \left[\frac{k_{s1} + (s-1)k_f - (s-1)\phi_1(k_f - k_{s1})}{k_{s1} + (s-1)k_f + \phi_1(k_f - k_{s1})} \right]$

mentioned that pure water has been used as the measured fluid in this investigation. Hybrid nanoparticles have also been created from GO (graphene oxide) and Cu (copper) nanoparticles. The innovation of this article, using a new approach, analyzes the heat transfer related to the flow of mixed nanofluid containing graphene oxide and copper particles in pure water, in a rotating system, and using the RBF method for the first time Investigates differential equations and simplified coupled equations.

2. Governing equations

Fig. 1 shows a steady hybrid nanofluid flow betwixt two equal straight surfaces. The liquid and the plates turn together

around the y-axis, which is typical to the plates by a precise velocity of Ω . Within the assumed Cartesian arranged framework, the x-axis is equal to the plate, the y-axis is opposite, and the z-axis is ordinary to the x-y plane. The top plate is subjected to a steady divider infusion velocity of $v_0 > 0$. The plates are arranged at $y = 0$ and $y = h$. The bottom plate is extended by two break- even with and inverse strengths, keeping up the area of the point $(0, 0, 0)$. A continuous flow injection with a velocity of v_0 is applied to the top plate. The Buongiorno demonstration is utilized to study about the impacts of Brownian movement and thermophoresis on stream, heat and mass exchange from a horizontal surface with a given sheet heat flux. The Buongiorno nanofluid model is used to study aspects of Brownian motion and thermophoresis. The equation applies to nanofluid flow and heat transfer. Nanoparticles concentrations and densities in mobile microbial fields are simplified using similarity transformations. The governing conditions in a pivoting outline of reference are [11,12,13,18]:

$$\left(\frac{\partial u^+}{\partial x}\right) + \left(\frac{\partial v^+}{\partial y}\right) + \left(\frac{\partial w^+}{\partial z}\right) = 0 \tag{1}$$

$$\rho_{hnf} \left(u \frac{\partial u^+}{\partial x} + v \frac{\partial u^+}{\partial y} + 2\Omega w^+ \right) + \frac{\partial p^+}{\partial x} - \mu_{hnf} \left(\frac{\partial^2 u^+}{\partial x^2} + \frac{\partial^2 u^+}{\partial y^2} \right) = 0 \tag{2}$$

Table 3 Shape factor coefficient for different nanoparticles' shapes [14].

Shapessofnanoparticle	S	Schematic
Spherical	3.0	
Brick	3.7	
Blade	8.6	

Table 4 Radial basic function categories [15–16].

Radialbasefunctionnames	NameAbbreviation	$\phi(\mathbf{r}), (\mathbf{r} \geq \mathbf{r})$	Stability
MultiQuadric	MQ	$\sqrt{1 + (\epsilon r)^2}$	Infinitely stable
InverseMultiQuadric	IMQ	$\frac{1}{\sqrt{1 + (\epsilon r)^2}}$	Infinitely stable
InverseQuadric	IQ	$\frac{1}{1 + (\epsilon r)^2}$	Infinitely stable
GeneralizedMultiQuadric	GMQ	$(1 + (\epsilon r)^2)^\beta$	Infinitely stable
Gaussian	GA	$e^{-(\epsilon r)^2}$	Infinitely stable
ThinPageSpline	TPS	$r^2 \log r$	Stable finite
Linear	LN	r	Stable finite
Cube	CU	r^3	Stable finite
SingleSentence	SS	r^{2k-1}	Stable finite

$$\rho_{hmf} \left(u^+ \frac{\partial v^+}{\partial y} \right) + \frac{\partial p^+}{\partial y} - \mu_{hmf} \left(\frac{\partial^2 v^+}{\partial x^2} + \frac{\partial^2 v^+}{\partial y^2} \right) = 0 \tag{3}$$

$$\rho_{hmf} \left(u^+ \frac{\partial w^+}{\partial x} + v^+ \frac{\partial w^+}{\partial y} - 2\Omega w^+ \right) - \mu_{hmf} \left(\frac{\partial^2 w^+}{\partial x^2} + \frac{\partial^2 w^+}{\partial y^2} \right) = 0 \tag{4}$$

$$\begin{aligned} & u^+ \frac{\partial T^+}{\partial x} + v^+ \frac{\partial T^+}{\partial y} + w^+ \frac{\partial T^+}{\partial z} \\ &= \alpha_{hmf} \left(\frac{\partial^2 T^+}{\partial x^2} + \frac{\partial^2 T^+}{\partial y^2} + \frac{\partial^2 T^+}{\partial z^2} \right) \\ &+ (\rho C_p)_{hmf} \left[D_B \left\{ \frac{\partial c^+}{\partial x} \cdot \frac{\partial T^+}{\partial x} + \frac{\partial c^+}{\partial y} \cdot \frac{\partial T^+}{\partial y} + \frac{\partial c^+}{\partial z} \cdot \frac{\partial T^+}{\partial z} \right\} \right. \\ &\left. + \left(\frac{D_T}{T_c} \right) \left\{ \left(\frac{\partial T^+}{\partial x} \right)^2 + \left(\frac{\partial T^+}{\partial y} \right)^2 + \left(\frac{\partial T^+}{\partial z} \right)^2 \right\} \right] \end{aligned} \tag{5}$$

$$\begin{aligned} & u^+ \frac{\partial c^+}{\partial x} + v^+ \frac{\partial c^+}{\partial y} + w^+ \frac{\partial c^+}{\partial z} \\ &= D_B \left(\frac{\partial^2 c^+}{\partial x^2} + \frac{\partial^2 c^+}{\partial y^2} + \frac{\partial^2 c^+}{\partial z^2} \right) \\ &+ \left(\frac{D_T}{T_o} \right) \left(\frac{\partial^2 T^+}{\partial x^2} + \frac{\partial^2 T^+}{\partial y^2} + \frac{\partial^2 T^+}{\partial z^2} \right) \end{aligned} \tag{6}$$

The velocities within the x , y , and z headings are spoken to by u^+ , v^+ , and w^+ . Additionally, ρ_{hmf} , D_B , μ_{hmf} , α_{hmf} , C , P^+ and T^+ , Ω are respectively for the hybridization nanofluids density, diffusion coefficient of the diffusing item, viscosity, thermal diffusivity, concentration, and the temperature and pressure of the revised liquid, and angular velocity accordingly. C_p is the specific heat transfer for hybrid nanoparticle. D_T is the specific diffusion coefficient of the diffusing thermal, and T_o

Table 5 Comparison of RBF and numerical results for dimensionless velocity profiles (f, g) when $\lambda = 3, \mathcal{R} = 0.5, K_r = 0.5, Sc = 0.5, \mathcal{N}_b = \mathcal{N}_t = 0.1$ and $Pr = 6$.

η	f			g		
	RBF	Numerical	Error	RBF	Numerical	Error
0	0	0	0	0	0	0
0.1	0.172245	0.166215	0.00603	0.128578	0.126548	0.00203
0.2	0.4629	0.443186	0.019714	0.234263	0.231194	0.003069
0.3	0.834293	0.799338	0.034955	0.308435	0.30569	0.002745
0.4	1.250991	1.204234	0.046757	0.346754	0.345512	0.001242
0.5	1.679914	1.62822	0.051694	0.348715	0.349592	-0.00088
0.6	2.09024	2.041955	0.048285	0.31716	0.320028	-0.00287
0.7	2.45324	2.415981	0.037259	0.257745	0.261763	-0.00402
0.8	2.742123	2.720457	0.021667	0.178399	0.182255	-0.00386
0.9	2.932	2.925178	0.006821	0.088815	0.091151	-0.00234
1.0	3	3	0	0	0	0

Table 6 Comparison of RBF and numerical results temperature profile (θ) and concentration profile (ϕ) when $\lambda = 3, \mathcal{R} = 0.5, K_r = 0.5, Sc = 0.5, \mathcal{N}_b = \mathcal{N}_t = 0.1$ and $Pr = 6$.

η	θ			ϕ		
	RBF	Numerical	Error	RBF	Numerical	Error
0	1	1	0	0	0	0
0.1	0.730801	0.732406	0.001606	1.05189	1.051502	-0.00039
0.2	0.478381	0.481764	0.003383	1.087083	1.085871	-0.00121
0.3	0.272049	0.276663	0.004613	1.076579	1.074605	-0.00197
0.4	0.13229	0.135564	0.003274	1.0006	1.000287	-0.00031
0.5	0.057328	0.055889	-0.00144	0.862569	0.867803	0.005234
0.6	0.02563	0.01933	-0.0063	0.687078	0.698491	0.011413
0.7	0.012339	0.005649	-0.00669	0.502926	0.515389	0.012464
0.8	0.003936	0.0014	-0.00254	0.326693	0.333892	0.007199
0.9	-0.00086	0.00027	0.001127	0.16026	0.161295	0.001035
1.0	-2.4e - 8	0.00118	0	0	0	0

is the temperature of the top plate. The nonappearance of $\left(\frac{\partial p^+}{\partial z}\right)$ in Eq. (4) infers a net cross-stream along the z- axle. Table 2 lists the thermophysical features of the working fluids and the nanomaterial's in combination, we found that graphene oxide and copper have improved thermophysical properties such as thermal conductivity, specific heat, viscosity and convective heat transfer compared to base liquids such as pure water. while Table 1 lists the thermal performance of a hybrid nanofluid, such as, C p, and k. The shape figure coefficients, as well as their relative shapes, are appeared in Table 3.

The pertinent border conditions are [11,12,13,18]:

$$\begin{cases} u^+ = ax, v^+ = 0, w^+ = 0, T^+ = T_h, c^+ = C_h @ y = 0 \\ u^+ = 0, v^+ = v_0, w^+ = 0, T = T_0, c^+ = C_0 @ y = +h \end{cases} \quad (7)$$

Non - dimensional factors are presented as takes after:

$$\begin{cases} \eta = \left(\frac{y}{h}\right) \\ u^+ = axf'(\eta) \\ v^+ = -ahf(\eta) \\ w^+ = axG(\eta) \\ \theta(\eta) = \left(\frac{T^+ - T_h}{T_0 - T_h}\right) \\ \phi(\eta) = \left(\frac{c^+ - C_h}{C_0 - C_h}\right) \end{cases} \quad (8)$$

Where a prime indicates separation about η . As a result, Eqs. (1) – (4) have the taking after non-dimensional designs:

$$-\left(\frac{1}{\rho_{hmf} \times h}\right) \left(\frac{\partial p^+}{\partial \eta}\right) = a^2 x \left[f' - ff'' - \frac{f'''}{\mathcal{R}} + \frac{2K_r}{\mathcal{R}} G \right] \quad (9)$$

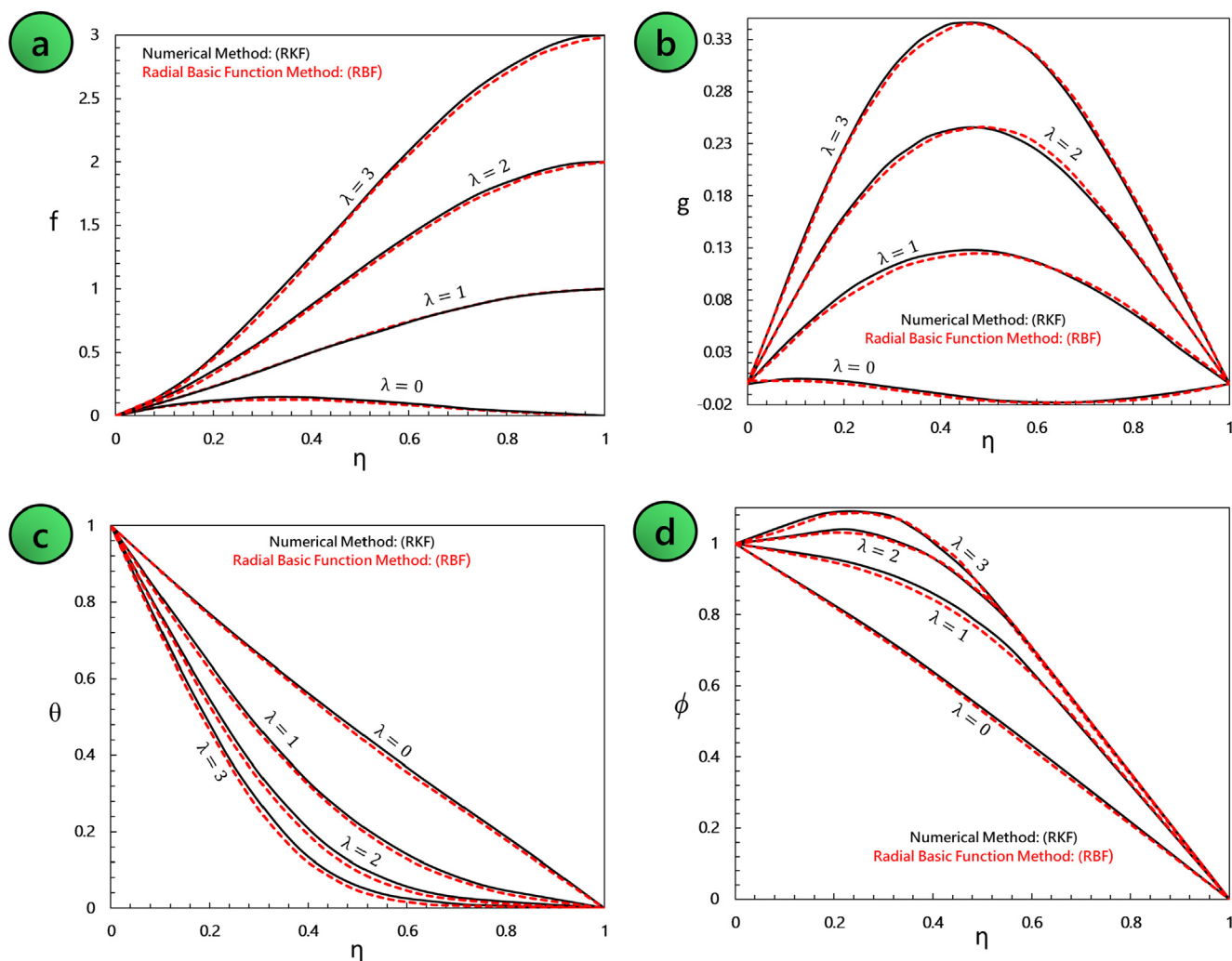


Fig. 2 Comparison of RBF and RKF Method for dimensionless velocity profiles (f, G), temperature profile (theta) and concentration profile (phi) when $\mathcal{R} = 0.5$, $K_r = 0.5$, $Sc = 0.5$, $N_b = N_i = 0.1$ and $Pr = 6$.

$$-\left(\frac{1}{\rho_{hmf} \times h}\right)\left(\frac{\partial p^+}{\partial \eta}\right) = a^2 h \left[ff' + \frac{1}{\mathcal{R}}f''\right] \tag{10}$$

$$\mathcal{G}'' - \mathcal{R}(f'\mathcal{G} - f\mathcal{G}') + 2K_r f' = 0 \tag{11}$$

And the non-dimensional amounts are characterized as:

$$\begin{cases} R = \left(\frac{ah^2}{\nu}\right) \\ K_r = \left(\frac{\Omega h^2}{\nu}\right) \end{cases} \tag{12}$$

K_r Is the Rotation quantity and R is the Reynolds number. With the help of Eq. (8), Eq. (9) may be communicated as:

$$f''' - \mathcal{R}[f^2 - ff''] - 2K_r^2 \mathcal{G} = A \tag{13}$$

When Eq. (13) is differentiated η , we get:

$$f^{iv} - \mathcal{R}(f'f'' - ff''') - 2K_r \mathcal{G}' = 0 \tag{14}$$

As a result, the following are the non-dimensional guiding formulas and initial conditions:

$$f^{iv} - \mathcal{R}(f'f'' - ff''') - 2K_r \mathcal{G}' = 0 \tag{15}$$

$$\mathcal{G}'' - \mathcal{R}(f'\mathcal{G} - f\mathcal{G}') + 2K_r f' = 0 \tag{16}$$

Eqs. (5) and (6) also become:

$$\theta'' + Pr\mathcal{R}f\theta' + \mathcal{N}_b\phi'\theta' + \mathcal{N}_t\theta^2 = 0 \tag{17}$$

$$\phi'' + \mathcal{R}.Scf\phi' + \left(\frac{\mathcal{N}_t}{\mathcal{N}_b}\right)\theta'' = 0 \tag{18}$$

Under the following boundary conditions:

$$\begin{cases} f = 0, f' = 1, G = 0, \theta = 1, \phi = 1 @ \eta = 0 \\ f = \lambda, f' = 0, G = 0, \theta = 0, \phi = 0 @ \eta = 1 \end{cases} \tag{19}$$

Additional non-dimensional quantities include:

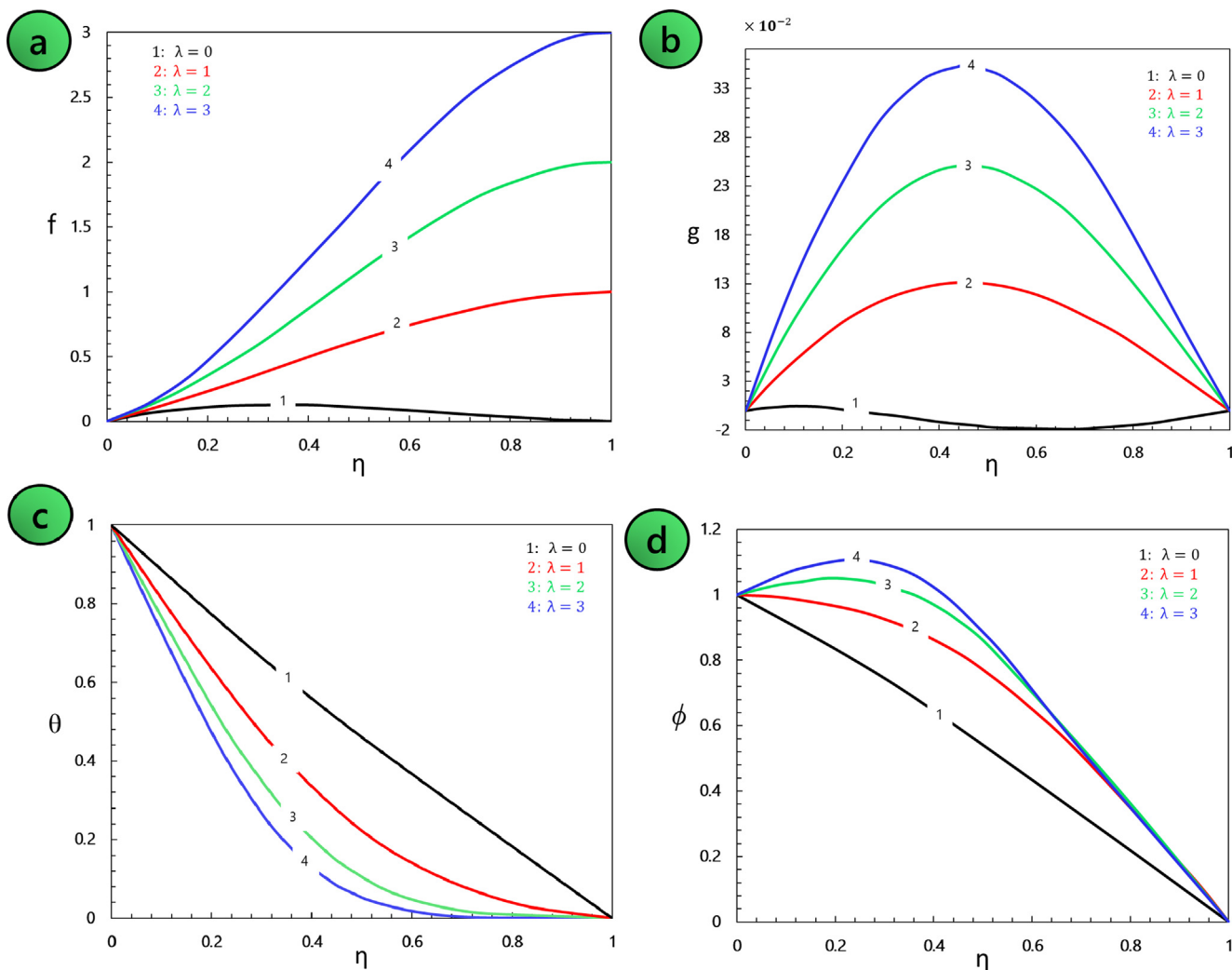


Fig. 3 Effect of injection quantity on (a, b) velocity profiles (f, \mathcal{G}), (c) temperature profile (θ) and (d) concentration profile (ϕ) when $\mathcal{R} = 0.5, K_r = 0.5, Sc = 0.5, \mathcal{N}_b = \mathcal{N}_t = 0.1$ and $Pr = 6$.

$$\left\{ \begin{array}{l} \lambda = \left(\frac{v_0}{ah}\right) \\ \mathcal{N}_b = \left(\frac{(\rho C)_p D_B C_h}{z(\rho C)_f}\right) \\ Pr = \left(\frac{\mu}{\rho_f \alpha}\right) \\ \mathcal{N}_t = \left(\frac{(\rho C)_p D_T T_h}{z(\rho C)_f T_c}\right) \\ Sc = \left(\frac{\mu}{\rho_f D}\right) \end{array} \right. \quad (20)$$

Following are the definitions of the coefficient of skin friction (C_f) and Nusselt number (Nu) along the stretched wall, N_b is the Brownian motion, Pr is the Prandtl number, Sc is the Schmidt number, and N_t is the thermophoretic effect.

$$\tilde{C}_f = \left(\frac{\mathcal{R}x}{h}\right) C_f = f''(0), Nu = -\theta'(0), Nu = \frac{hl}{k} \quad (21)$$

The average Nusselt number is the normal of the nearby Nusselt numbers over the heat exchange surface. Subsequently, its esteem depends on the heat exchange geometry

or surface zone. The nature of the stream administration or space isn't an impediment in utilizing the normal Nusselt number as the heat exchange coefficient.

3. Basic idea of radial basis function method (RBFM) [24–25]:

The radial basis subordinate strategy is one of the superlative realistic approaches to multivariate approximation in novel theorization, and it is utilized for extraordinary exactness and adaptability In the geometry of the dimensional autonomy problem and its simple implementation. F is radial when:

$$F(x) = F(y) \iff \|x\| = \|y\| \quad (22)$$

If this feature holds, the values of $F(x)$ depend only on $\|x\|$. As a result, we'll be in a position to...

$$F(x) = f(\|x\|^2) \quad (23)$$

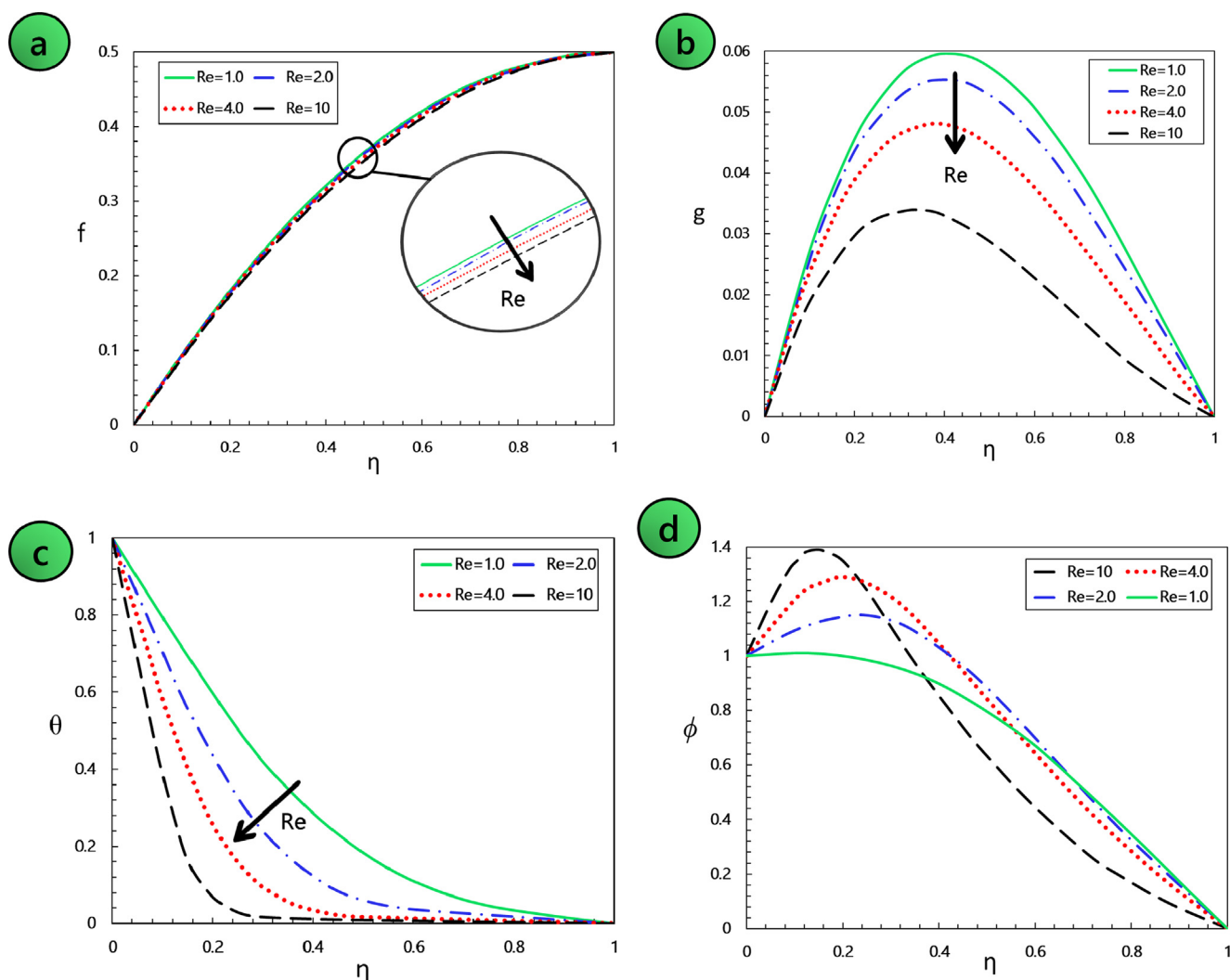


Fig. 4 Effect of Reynolds numerical on velocity profiles (f, g), temperature profile (θ) and concentration profile (ϕ) when $\lambda = 0.5$, $K_r = 0.5$, $\mathcal{N}_b = \mathcal{N}_t = 0.1$ and $Pr = 6$.

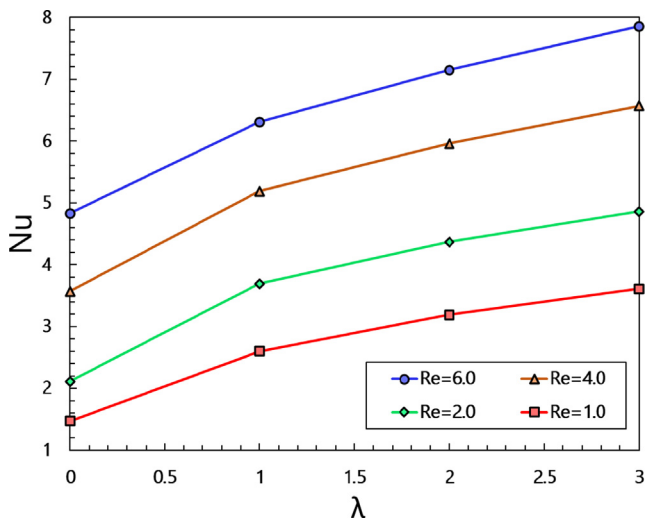


Fig. 5 Effects of injection quantity and Reynolds number on Nusselt number when $K_r = 0.5$, $\mathcal{R} = 0.5$, $\mathcal{N}_b = \mathcal{N}_t = 0.1$ and $Pr = 10$.

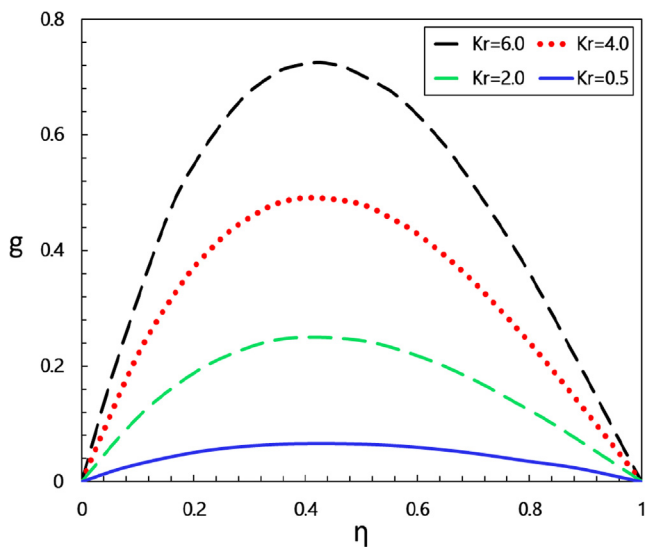


Fig. 6 Effect of Rotation quantity on velocity profile when $\mathcal{R} = 0.5$, $\lambda = 0.5$, $Sc = 0.5$, $\mathcal{N}_b = \mathcal{N}_t = 0.1$.

A few of the foremost broadly utilized outspread premise capacities are included in Table 4.

The radial basis functions are divided into two main groups, as exhibited in Table 4.

Infinitely stable radial base functions

These functions are endlessly differentiable and the state quantity has greatly affected them.

Finitely stable radial base functions

Fundamental capacities in this grade are not perpetually differentiable. These capacities don't have accessible amounts and are less accurate than the actual capacities within the to begin with segment. The persuasion of the object and the sum of required exactness ought to decide the foremost appropriate alternative.

4. Solution of the problem

By selecting a suitable radial basis function from Table 4, Eqs. (15) – (18) might be solved using the boundary conditions of Eq. (19). Since the equation has no harmonic response and the response is the result of this function, a Gaussian function is applied as the radial basis function.

$$\Psi(\eta) = \exp(-Y \times (\eta - S)^2) \tag{24}$$

For velocity, temperature and concentration functions:

$$\begin{cases} f(\eta) = \sum_{i=0}^2 a_i \exp(-Y \times (\eta - S_i)^2) \\ G(\eta) = \sum_{i=0}^2 b_i \exp(-Y \times (\eta - S_i)^2) \\ \theta(\eta) = \sum_{i=0}^2 c_i \exp(-Y \times (\eta - S_i)^2) \\ \phi(\eta) = \sum_{i=0}^2 z_i \exp(-Y \times (\eta - S_i)^2) \end{cases} \tag{25}$$

in the aforementioned equation $n = 2$, and S_i represents radial basis function centers.

$$\begin{cases} S_0 = 0.2 \\ S_1 = 0.4 \\ S_2 = 0.6 \end{cases} \tag{26}$$

Y is the adjustment coefficient (shape quantity) and equivalent to 0.01. consequently, the velocity, temperature, and concentration functions may be described in greater detail as:

Table 7 Effect of Rotation quantity on Nusselt numerical when $\mathcal{R} = 1$, $\mathcal{R} = 0.5$, $\mathcal{N}_b = \mathcal{N}_t = 0.1$.

	$K_r = 0.5$	$K_r = 2.0$	$K_r = 4.0$	$K_r = 6.0$
λ	Nu			
1	2.63360451931608	2.63351840850970	2.63350692873705	2.63429550500028
2	3.27111121892871	3.27175258536992	3.27418584843087	3.27942176227005
3	3.74580608261866	3.74607855447263	3.74742657801822	3.75117550119

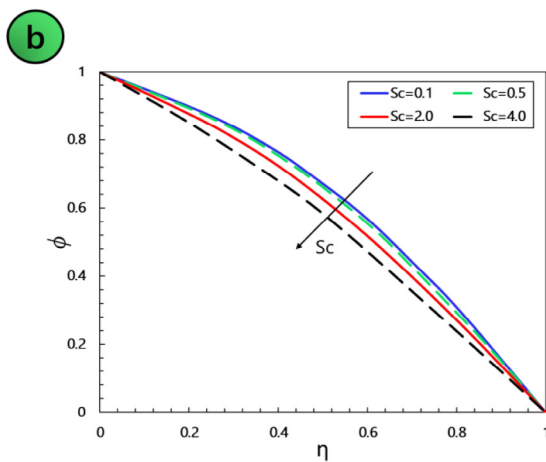
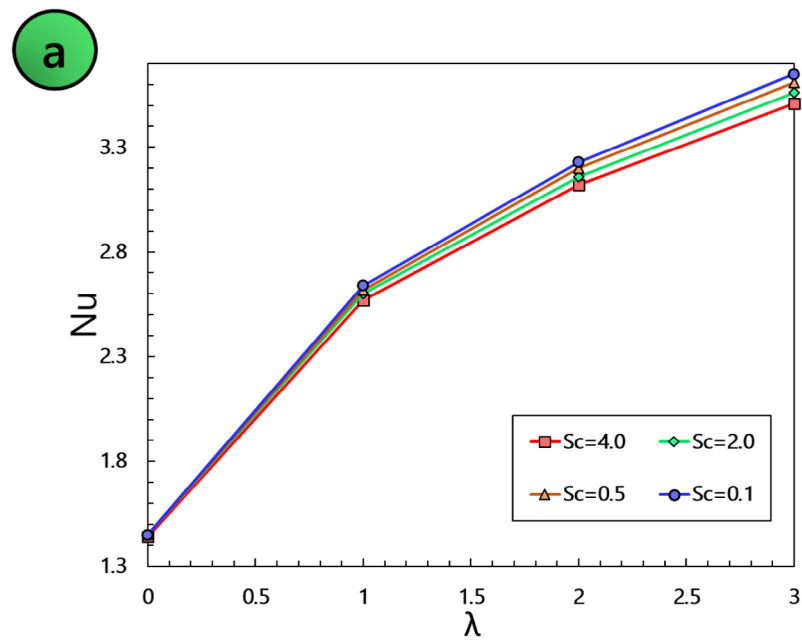
$$f(\eta) = a_0 \times e^{(-0.01 \times (\eta-0.2)^2)} + a_1 \times e^{(-0.01 \times (\eta-0.4)^2)} + a_2 \times e^{(-0.01 \times (\eta-0.6)^2)} \tag{27}$$

$$\phi(\eta) = z_0 \times e^{(-0.01 \times (\eta-0.2)^2)} + z_1 \times e^{(-0.01 \times (\eta-0.4)^2)} + z_2 \times e^{(-0.01 \times (\eta-0.6)^2)} \tag{30}$$

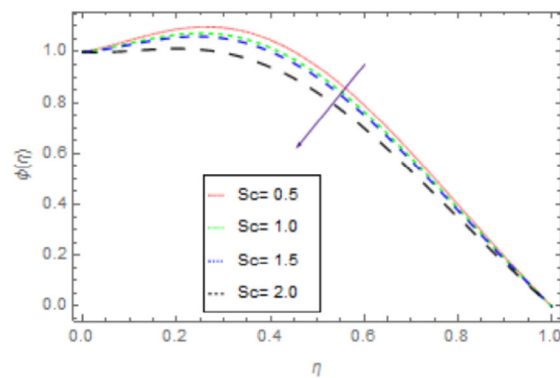
$$\mathcal{G}(\eta) = b_0 \times e^{(-0.01 \times (\eta-0.2)^2)} + b_1 \times e^{(-0.01 \times (\eta-0.4)^2)} + b_2 \times e^{(-0.01 \times (\eta-0.6)^2)} \tag{28}$$

$$\theta(\eta) = c_0 \times e^{(-0.01 \times (\eta-0.2)^2)} + c_1 \times e^{(-0.01 \times (\eta-0.4)^2)} + c_2 \times e^{(-0.01 \times (\eta-0.6)^2)} \tag{29}$$

by Inserting Eqs. (26) – (30) into Eqs. (15) – (18) and taking the appropriate boundary conditions into consideration, We can find the undetermined value of the radial basis function. We have the values of $\mathcal{N}_b = 0.1$, $\mathcal{N}_t = 0.1$, $\mathcal{R} = 0.8$, $K_r = 0.5$, $Pr = 6$, $Sc = 0.6$ for specific problem characteristics. Finally, the $f(\eta)$, $\mathcal{G}(\eta)$, $\theta(\eta)$ and $\phi(\eta)$ functions can be calculated:



a) Present work



b) Zahir Shah et al.[18] works

Fig. 7 Effect of Schmidt number on concentration profile and Nusselt number for present work (left image) and Zahir Shah work [18] (right image) when (a) $\mathcal{R} = 1$, $\lambda = 0.5$, $K_r = 0.3$, $\mathcal{N}_b = \mathcal{N}_t = 0.3$; (b) $K_r = 0.3$, $\mathcal{N}_b = \mathcal{N}_t = 0.3$, $\mathcal{R} = 1$.

$$f(\eta) = -62649.95738 \times e^{(-0.01 \times (\eta-0.2)^2)} + 125199.9645 \times e^{(-0.01 \times (\eta-0.4)^2)} - 62599.85666 \times e^{(-0.01 \times (\eta-0.6)^2)} \quad (31)$$

$$\mathcal{G}(\eta) = 1.262178885 \times 10^6 \times e^{(-0.01 \times (\eta-0.2)^2)} - 2.522341610 \times 10^6 \times e^{(-0.01 \times (\eta-0.4)^2)} + 1.261167025 \times 10^6 \times e^{(-0.01 \times (\eta-0.6)^2)} \quad (32)$$

$$\theta(\eta) = 20781.34168 \times e^{(-0.01 \times (\eta-0.2)^2)} - 41278.62785 \times e^{(-0.01 \times (\eta-0.4)^2)} + 20514.32284 \times e^{(-0.01 \times (\eta-0.6)^2)} \quad (33)$$

$$\phi(\eta) = 46.23730165 \times e^{(-0.01 \times (\eta-0.2)^2)} - 33.40192956 \times e^{(-0.01 \times (\eta-0.4)^2)} + 17.42383508 \times e^{(-0.01 \times (\eta-0.6)^2)} \quad (34)$$

Tables 5 - 6 offer a comparison of the RBF approach with the numerical method (Runge-Kutte 4th) (6). All the related calculations and simplifications implemented in this step are drawn in the uncertain analysis diagram in Fig. 12.

5. Results

This investigation investigated the half-breed nanofluid stream and heat exchange in a turning framework. For this problem, the radial basis function approach (RBF) was utilized, and to ensure the exactness of the progress comes about, we compared them to numerical sequences obtained using the fourth-order Runge-Kutta-Fehlberg methodology. (See Fig. 2, Table 5 and Table 6). This comparison reveals a high level of agreement. In this situation, it shows that the RBF solution is trustworthy. The affect of the infusion amount on velocity, temperature, and concentration is additionally shown in Figs. 2 and 3, where the velocity profiles is proportional to the injection value. Also, for validation with the work of others, Fig. 7 compares the changes in nanofluid concentration between the present work and the research of Dr. Zahir and his colleagues. According to the 2 graphs, the convergence between the results of both articles are proportional to each other, which shows the correctness of the solution of the present work. As the injection quantity is raised, the velocity sec-

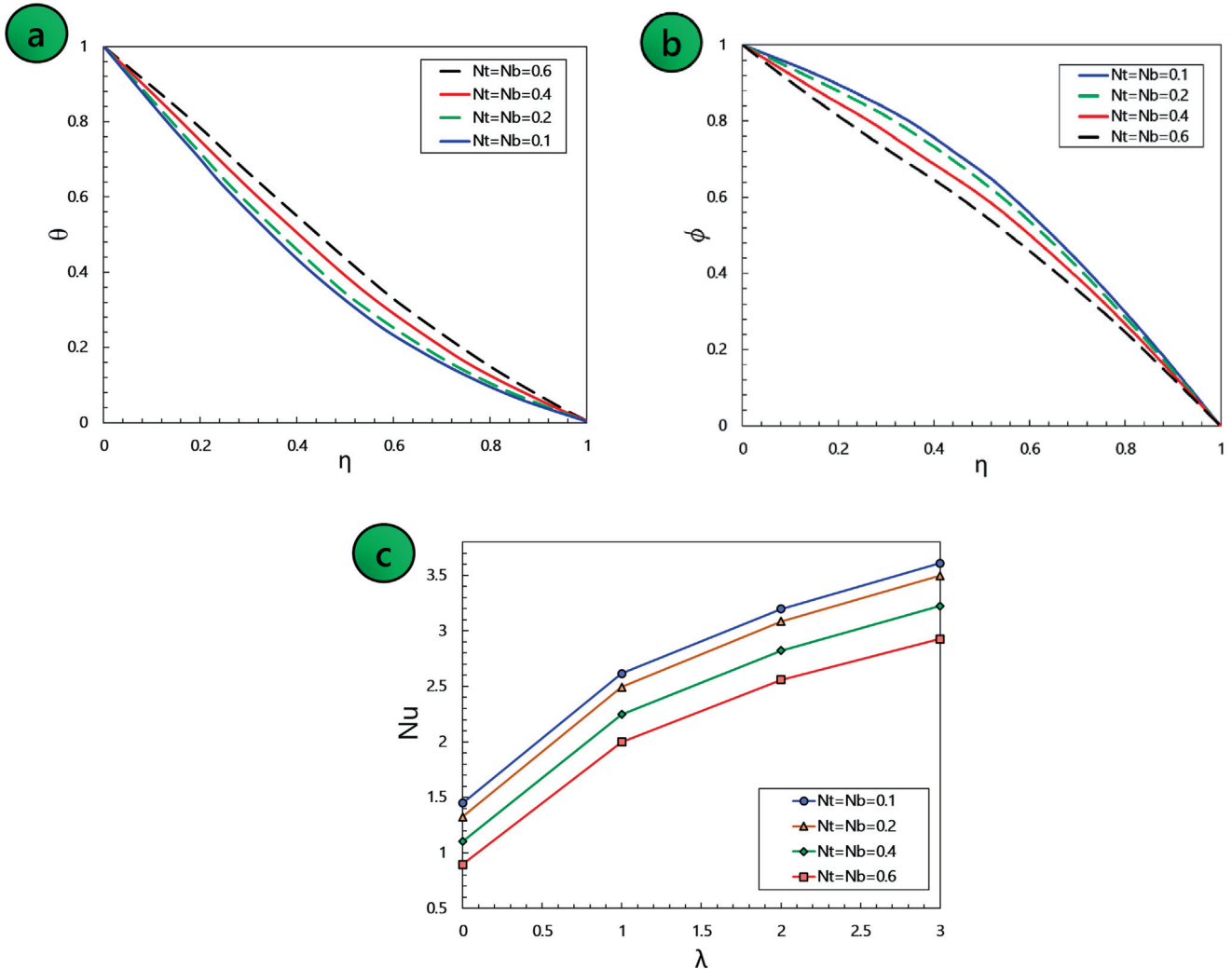


Fig. 8 Effects of Brownian quantity and thermophoretic quantity on temperature, concentration profile and Nusselt numerical when (a, b) $\mathcal{R} = 0.5$, $\lambda = 0.5$, $K_r = 0.5$, $Sc = 0.5$; (c) $K_r = 0.5$, $Sc = 0.1$, $\mathcal{R} = 1$ and $Pr = 6$.

tions also rise. However, as the injection quantity is grown, the temperature profile drops, while the concentration profile follows the opposite behavior. Fig. 4 demonstrates the impacts of the Reynolds number and injection quantity on velocity, temperature and concentration, while Fig. 5 depicts the influence of the Reynolds number and injection quantity on the Nusselt number. As can be observed, the Nusselt number rises as the injection quantity climbs, so the heat transfer ratio will increase as the Nusselt number rises. According to Fig. 4, with the increment of Reynolds number, the amount of heat transfer decreases greatly, and with the decrease of heat flows from the surfaces, the flow rate of fluid and nanofluid decreases. However, the concentration of nanomaterials reaches its maximum value as the Reynolds number increases. Reynolds number is important unit quantity that is used in fluid mechanics to predict the flow pattern. This number is the ratio of shear force to viscous force. As the velocity and Reynolds number increase, the Nusselt number will also increase according to

picture number 5. As the Nusselt number increases, more heat will be transferred between the nanofluid and the plates. The values of fluid suction and boiling on the top of the page vary from 0 to 3 for all types of Nusselt numbers, so that for a constant Reynolds number, the faster the fluid suction and boiling occurs, the larger the Nusselt number will be. Fig. 6 shows the changes of the transverse velocity variable in relation to the changes in the rotation parameter of the upper plate. As the value of rotation of the plate increases in the vertical direction, the transverse velocity of the nanofluid between the force plates increases across the plate. The impacts of the revolution amount on the velocity profile and Nusselt number are outlined in Fig. 6 and Table 7, separately. The transverse velocity rises when the revolution amount is upgraded. In Table No. 7, as the suction and flow of the fluid increase, the measures of the Nusselt number parameter for several parameters of the rotating plates increase. A Schmidt number is a no- dimensional number that describes the ratio of momentum diffusion

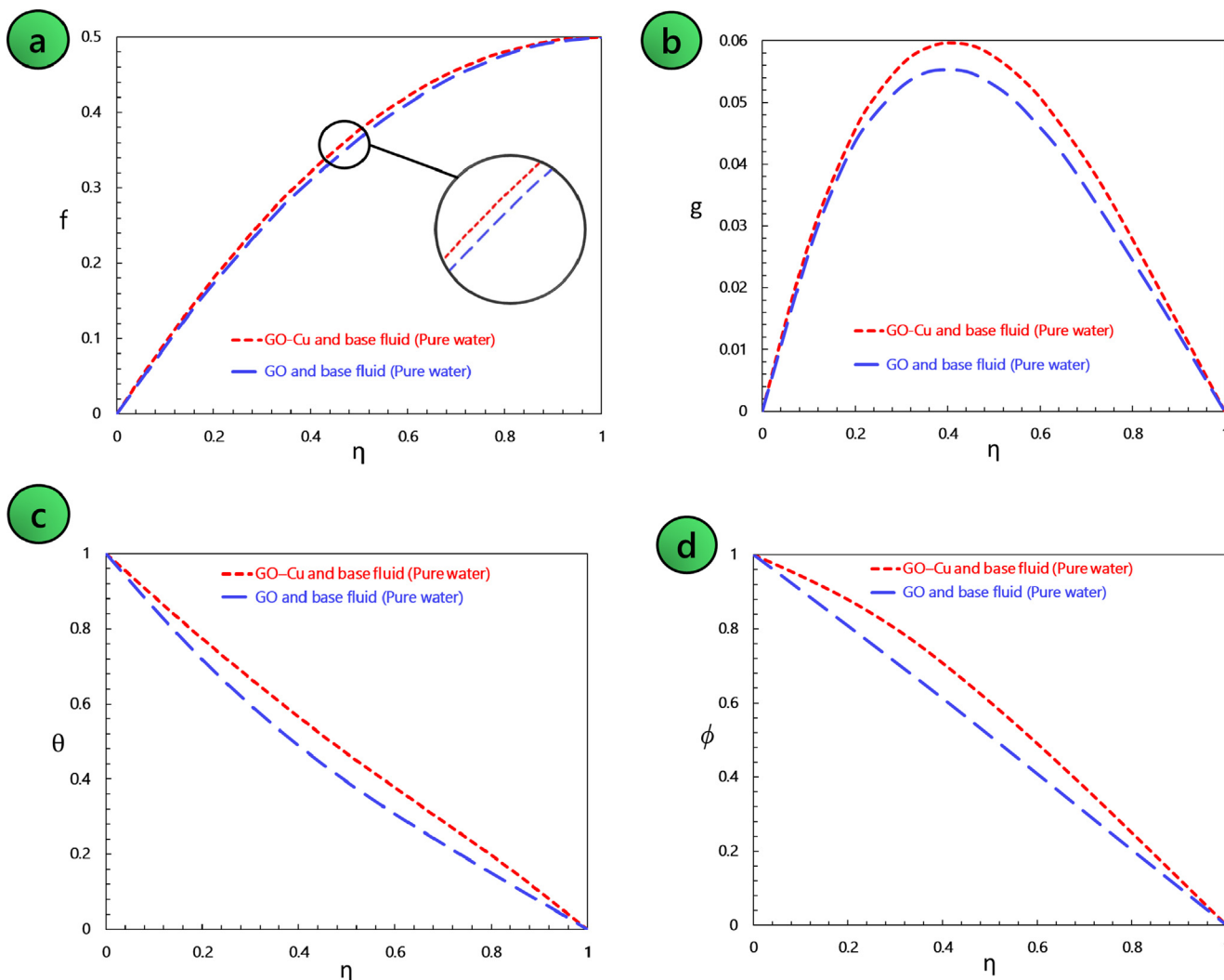


Fig. 9 Comparison of velocity profiles (f, g), temperature profile (θ) and concentration profile (ϕ) between hybrid and single nanoparticles when $\mathcal{R} = 0.5, \lambda = 0.5, K_r = 0.5, Sc = 0.5, \mathcal{N}_b = \mathcal{N}_t = 0.1$ and $Pr = 10$.

to mass diffusion in a fluid. It is utilized to describe fluid motion that simultaneously involves mass diffuse convective and momentum convective. Fig. 7 appears the impact of diverse amounts of Schmidt number on changes in Nusselt number and concentration. The concentration segment decreases as the Schmidt number rises. As the values of the Schmidt number decrease, the values of the Nusselt number parameter will decrease insignificantly, which causes the heat transfer to decrease. Fig. 8 depicts the impact of Brownian and thermophoretic motions on temperature, concentration segments, and Nusselt number. Brownian motion is the random movement of particles as a consequence of collisions with surrounding gas molecules. Diffusion migration is the move-

ment of groups of particles caused by concentration gradients. This movement is always flowing from high density to low density. Thermophoresis is a phenomenon examined in moving particle mixtures, where different types of particles respond differently to the forces of temperature gradients. This phenomenon tends to move lighter molecules to higher temperature regions and heavier molecules to lower temperature regions. By equating the numerical values of Brownian force and thermophoretic coefficient parameters in Fig. 8, it is concluded that as these values increase from 0.1 to 0.6, the amount of heat transfer and Nusselt number also reaches its maximum values, but the nanofluid concentration values are decreasing. The Nusselt number decreases as the thermophoretic quantity and Brownian motion increase. Fig. 9 provides an assessment of the effects of hybrid nanoparticles vs single nanoparticles on velocity, temperature, and concentration profiles. When hybrid nanoparticles are utilized, this efficiency is increased by 8 percent, leading in an improvement in the temperature profile. Hybrid nanofluids are gotten by including two or more distinctive nanoparticles in the base liquids in arrange to extent, which for the most part renders higher k than watched in immaculate liquids or single- molecule nanofluids. Hybrid nanofluids have been found to have upgraded thermophysical properties such as heat conductivity, heat diffusivity, thickness, and convective heat exchange coefficients compared to those of base liquids like oil or water. Fig. 10 demonstrates the influx of the solid volume fraction of hybrid nanofluid on temperature distribution and velocity components. The three solid volume fractions of hybrid nanofluid ($\phi = 1\%$, 2% , 3%) were investigated in this figure, and it was discovered that the ascending trend of ϕ had a direct influence on raising the temperature distribution and velocity. Because nanoparticles have more surface area for heat transfer, the heat transfer coefficient of nanofluid is higher than normal fluid. As a result, with the increase in the volume percentage of Nano, heat transfer, temperature distribution and nanofluid velocity increase. The thermal conductivity and dynamic viscosity of a nanofluid can be affected by the shape of the nanoparticle. Consequently, in Fig. 11, we sought to investigate the various morphologies of nanoparticles. As seen in Fig. 11, the influence of the shape factor on velocity sections (f, g) and temperature section (θ) is apparent. When the shape factor increases from 3 to 8.6, the f, g and θ profiles are reduced by 18, 64, and 21 percent, respectively. Shape factor is characterized as the proportion of the plastic moment and the abdicate moment of the segment. It may be a work of the cross-section frame or shape and is spoken to by S . The lower the plastic moment of the object used, the faster the velocity of the nanofluid passing between the 2 plates and the increase of the boundary layer, the same points apply to heat. Shape calculates (SF) is the non-dimensional proportion of the parcel edge (P) squared, separated by the parcel region (A). According to the above objects and considering that the surface area of the cylinder is more than the others, it has lower values of the parameter s , which causes an increase in the velocity and temperature of the nanofluid bit and the base fluid and sheets.

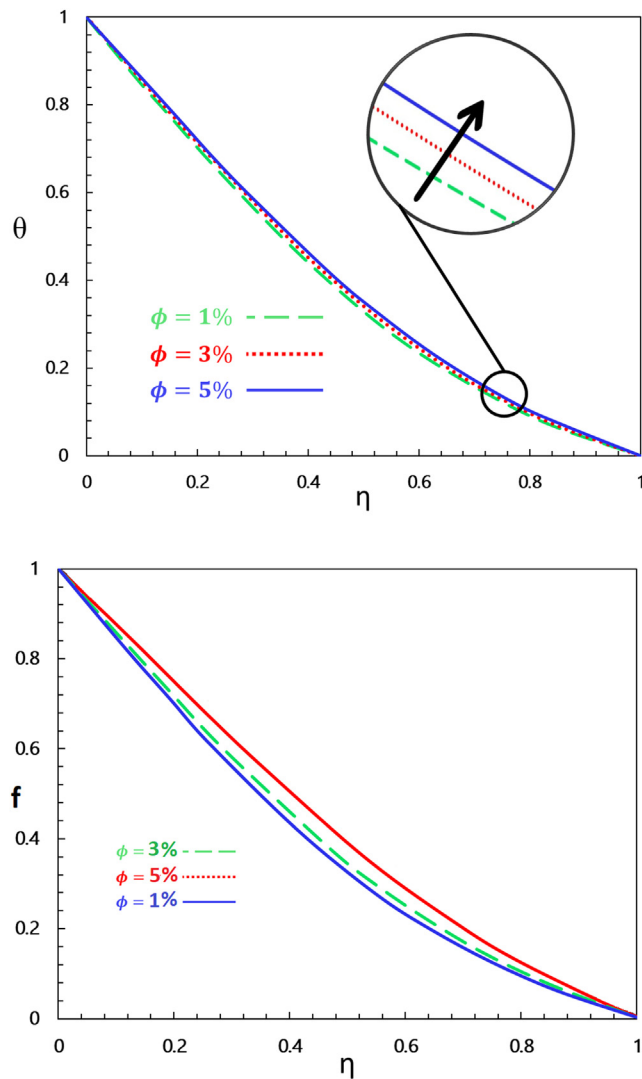


Fig.10 Impacts of solid volume fraction on the temperature and velocity profile (θ) when $\mathcal{R} = 0.5$, $\lambda = 0.5$, $K_r = 0.5$, $Sc = 0.5$, $\mathcal{N}_b = \mathcal{N}_t = 0.1$ and $Pr = 6$.

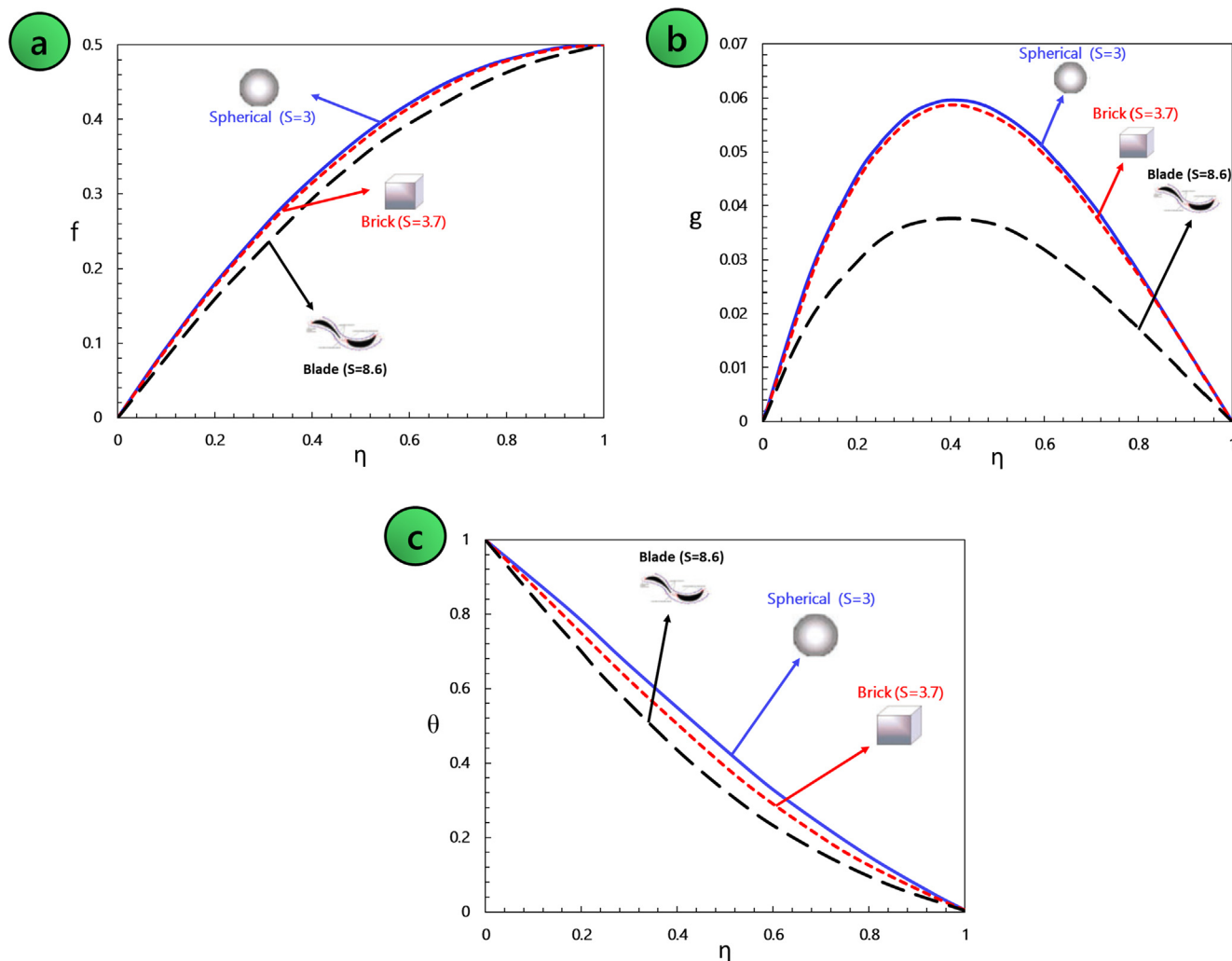


Fig.11 The influence of shape factor coefficient on velocity profiles (f , g) and temperature profile (θ) when $\mathcal{R} = 0.5$, $\lambda = 0.5$, $K_r = 0.5$, $Sc = 0.5$, $\mathcal{N}_b = \mathcal{N}_t = 0.1$ and $Pr = 6$.

6. Conclusions

In later a long time, the study of thermal and mass transmission in rotational systems has become increasingly significant. As a result, numerous researchers have attempted to solve the governing equations of these types of problems analytically. In this paper, by using a novel approach, the heat transmission related to the hybrid nanofluid flow containing grapheme oxide and copper particles in pure water, which is located in a rotating system, is analyzed. The RBF methodology was utilized to solve the equations, and the outcomes were compared to those obtained using the Runge –Kutta –Fehlberg numerical course. One of the most important applications of the RBF method in this article is the use of the radial substrategy as one of the most important events for multivariate strengthening in engineering science theories, and it has high accuracy and consistency in geometry. Moreover, the impact of factors such as nanofluid volume fraction and nanoparticle shape factor on non-dimensional velocity and temperature dis-

tribution for single and hybrid nanofluids has been reported. As the main outcome, the results demonstrate that, Nusselt number, Reynolds number and Injection quantity directly communicate per each other while Nusselt number has an inverse communication per Schmidt number, Thermophoretic quantity, Rotation quantity and Brownian quantity. The following are some of the key significant outcomes of this paper:

- The Nusselt number rises as the Reynolds number rises, but when the Schmidt number, Brownian quantity, and thermophoretic quantity increase, the trend falls.
- With increasing thermophoretic and Brownian quantities, the width of the concentration boundary layer is reduced.
- When the rotation quantity is increased, the transverse velocity grows. As the rotation quantity rises, the width of the heat boundary layer reduces, but the Nusselt number goes up.
- The increasing trend of ϕ has a positive impact on the temperature variation growing.

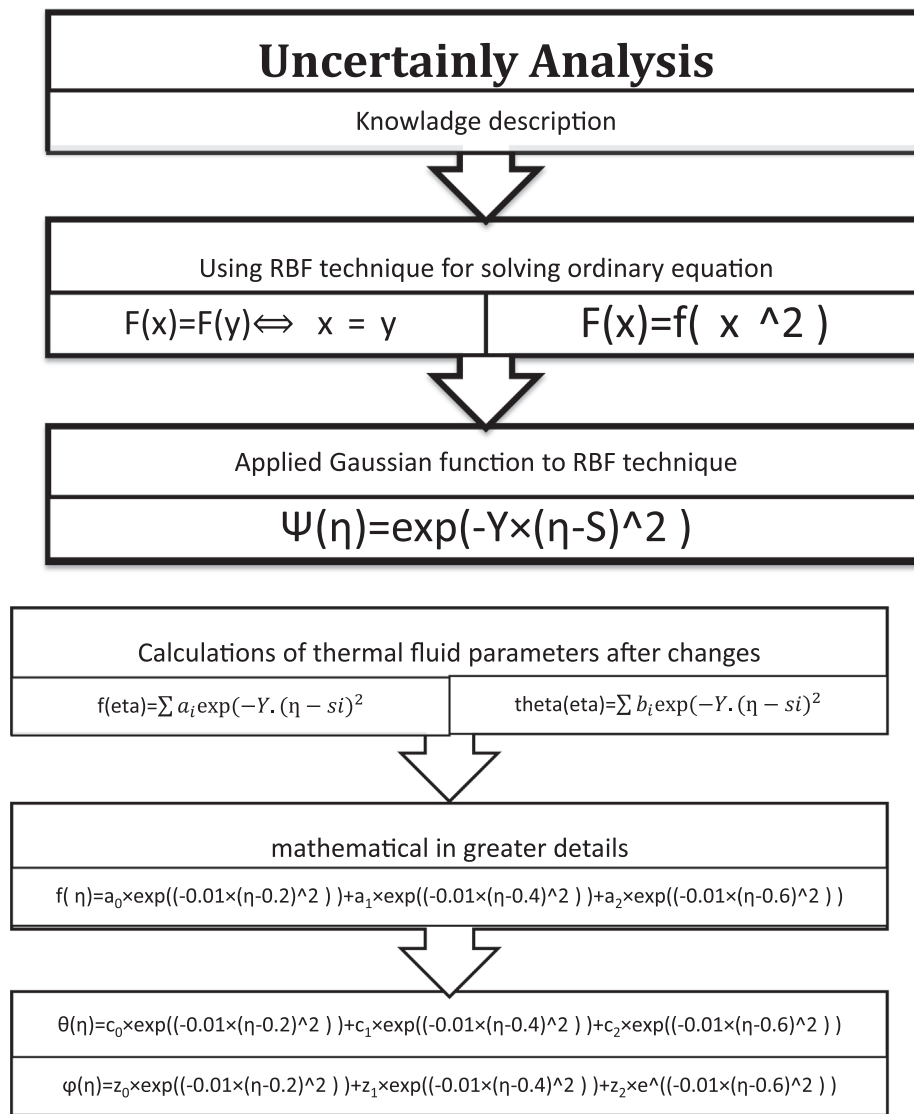


Fig.12 The Uncertainty Analysis chart.

Declaration of Competing Interest

The authors declare that they have no known competing financial interests or personal relationships that could have appeared to influence the work reported in this paper. This article has not received any funding.

References

- [1] A.J. Chamkha, A.S. Dogonchi, D.D. Ganji, Magneto-hydrodynamic flow and heat transfer of a hybrid nanofluid in a rotating system among two surfaces in the presence of thermal radiation and Joule heating, *AIP Adv.* 9 (2) (2019) 025103.
- [2] S.M. Hussain et al, Free convective heat transfer with hall effects, heat absorption and chemical reaction over an accelerated moving plate in a rotating system, *J. Magn. Magn. Mater.* 422 (2017) 112–123.
- [3] M. Turkyilmazoglu, Fluid flow and heat transfer over a rotating and vertically moving disk, *Phys. Fluids* 30 (6) (2018) 063605.
- [4] M. Turkyilmazoglu, Suspension of dust particles over a stretchable rotating disk and two-phase heat transfer, *Int. J. Multiph. Flow* 127 (2020) 103260.
- [5] Z. Shah et al, Three-dimensional third grade nanofluid flow in a rotating system between parallel plates with Brownian motion and thermophoresis effects, *Results Phys.* 10 (2018) 36–45.
- [6] Z. Shah et al, Radiative heat and mass transfer analysis of micropolar nanofluid flow of Casson fluid between two rotating parallel plates with effects of Hall current, *J. Heat Transfer* 141 (2019) 2.
- [7] S. Xun et al, Bioconvection in rotating system immersed in nanofluid with temperature dependent viscosity and thermal conductivity, *Int. J. Heat Mass Transf.* 111 (2017) 1001–1006.
- [8] O. Pourmehran et al, Rheological behaviour of various metal-based nano-fluids between rotating discs: a new insight, *J. Taiwan Inst. Chem. Eng.* 88 (2018) 37–48.
- [9] C. Yin et al, Flow and heat transfer of nanofluids over a rotating disk with uniform stretching rate in the radial direction, *Propul. Power Res.* 6 (1) (2017) 25–30.
- [10] K.A. Abro et al, Enhancement of heat transfer rate of solar energy via rotating Jeffrey nanofluids using Caputo-Fabrizio

- fractional operator: an application to solar energy, *Energy Rep.* 5 (2019) 41–49.
- [11] S. Kadri, R. Mehdaoui, M. Elmir, A Vertical magneto-convection in square cavity containing a Al_2O_3 + water nanofluid: cooling of electronic compounds, *Energy Procedia* 18 (2012) 724–732.
- [12] Z. Shah et al, Hall effect on Titania nanofluids thin film flow and radiative thermal behavior with different base fluids on an inclined rotating surface, *AIP Adv.* 9 (5) (2019) 055113.
- [13] M. Jawad et al, Insight into the dynamics of second grade hybrid radiative nanofluid flow within the boundary layer subject to Lorentz force, *Sci. Rep.* 11 (1) (2021) 1–14.
- [14] M.D. Massoudi, M.B.B. Hamida, MHD natural convection and thermal radiation of diamond–water nanofluid around rotating elliptical baffle inside inclined trapezoidal cavity, *Eur. Phys. J. Plus* 135 (11) (2020) 1–24.
- [15] M. Aslefallah, E. Shivanian, A nonlinear partial integro-differential equation arising in population dynamic via radial basis functions and theta-method, *J. Mathematics and Comput. Sci.* 13 (1) (2014) 14–25.
- [16] Fabien, Maurice S. “A Radial Basis Function (RBF) Method for the Fully Nonlinear 1D Serre Green-Naghdi Equations.” arXiv preprint arXiv:1407.4300 (2014).
- [17] T. Hayat et al, Entropy generation analysis for peristaltic flow of nanoparticles in a rotating frame, *Int. J. Heat Mass Transf.* 108 (2017) 1775–1786.
- [18] Z. Shah et al, Effects of hall current on steady three-dimensional non-newtonian nanofluid in a rotating frame with Brownian motion and thermophoresis effects, *J. Eng. Technol* 6 (280) (2017) e296.
- [19] Z. Shah et al, The electrical MHD and hall current impact on micropolar nanofluid flow between rotating parallel plates, *Results Phys.* 9 (2018) 1201–1214.
- [20] Y. Dou et al, The effect of surface functional groups on the wettability of graphene oxide coated alumina substrate: molecular dynamics simulations, *J. Mol. Liq.* 366 (2022) 120268.
- [21] A. Vărdaru et al, Aqueous hybrid nanofluids containing silver-reduced graphene oxide for improving thermo-physical properties, *Diam. Relat. Mater.* (2023) 109688.
- [22] P. Pasha et al, The application of analytical methods in the investigation effects of Magnetic parameter and Brownian motion on the fluid flow between two equal plates, *Int. J. Eng.* 34 (10) (2021) 2341–2350.
- [23] P. Pooya, S. Mirzaei, M. Zarinfar, Application of numerical methods in micropolar fluid flow and heat transfer in permeable plates, *Alex. Eng. J.* 61 (4) (2022) 2663–2672.
- [24] E. Tayari et al, Analytical solution of electromagnetic force on nanofluid flow with brownian motion effects between parallel disks, *Int. J. Eng.* 35 (8) (2022) 1651–1661.
- [25] E. Tayari et al, Investigation of hybrid nanofluid SWCNT–MWCNT with the collocation method based on radial basis functions, *Eur. Phys. J. Plus* 138 (1) (2023) 3.
- [26] S. Dinarvand, Nodal/saddle stagnation-point boundary layer flow of CuO – Ag /water hybrid nanofluid: a novel hybridity model, *Microsyst. Technol.* 25 (7) (2019) 2609–2623.
- [27] M. Izady et al, Flow of aqueous Fe_2O_3 – CuO hybrid nanofluid over a permeable stretching/shrinking wedge: a development on Falkner-Skan problem, *Chin. J. Phys.* 74 (2021) 406–420.
- [28] S. Dinarvand, A.M. Nejad, Off-centered stagnation point flow of an experimental-based hybrid nanofluid impinging to a spinning disk with low to high non-alignments, *Int. J. Numer. Meth. Heat Fluid Flow* 32 (8) (2021) 2799–2818.
- [29] H. Berrehal, S. Dinarvand, I. Khan, Mass-based hybrid nanofluid model for entropy generation analysis of flow upon a convectively-heated moving wedge, *Chin. J. Phys.* 77 (2022) 2603–2616.
- [30] S. Dinarvand et al, MHD flow of MgO – Ag /water hybrid nanofluid past a moving slim needle considering dual solutions: an applicable model for hot-wire anemometer analysis, *Int. J. Numer. Meth. Heat Fluid Flow* 32 (2) (2022) 488–510.
- [31] F. Hoseininejad, S. Dinarvand, M.E. Yazdi, Manninen’s mixture model for conjugate conduction and mixed convection heat transfer of a nanofluid in a rotational/stationary circular enclosure, *Int. J. Numer. Meth. Heat Fluid Flow* 31 (5) (2021) 1662–1694.
- [32] A. Ghasemian et al, Unsteady general three-dimensional stagnation point flow of a Maxwell/Buongiorno non-Newtonian nanofluid, *Journal of Nanofluids* 8 (7) (2019) 1544–1559.
- [33] B. Jabbaripour et al, Aqueous aluminium–copper hybrid nanofluid flow past a sinusoidal cylinder considering three-dimensional magnetic field and slip boundary condition proceedings of the institution of mechanical engineers, Part E, *J. Process Mechanical Eng.* (2021), 09544089211046434.
- [34] A. Bhattad, J. Sarkar, P. Ghosh, Discrete phase numerical model and experimental study of hybrid nanofluid heat transfer and pressure drop in plate heat exchanger, *Int. Commun. Heat Mass Transfer* 91 (2018) 262–273.
- [35] A. Bhattad, J. Sarkar, P. Ghosh, Experimentation on effect of particle ratio on hydrothermal performance of plate heat exchanger using hybrid nanofluid, *Appl. Therm. Eng.* 162 (2019) 114309.
- [36] A. Bhattad, J. Sarkar, P. Ghosh, Hydrothermal performance of different alumina hybrid nanofluid types in plate heat exchanger: experimental study, *J. Therm. Anal. Calorim.* 139 (2020) 3777–3787.
- [37] A. Bhattad, J. Sarkar, P. Ghosh, Energetic and exergetic performances of plate heat exchanger using brine-based hybrid nanofluid for milk chilling application, *Heat Transfer Eng.* (2019).
- [38] A. Bhattad, J. Sarkar, Effects of nanoparticle shape and size on the thermohydraulic performance of plate evaporator using hybrid nanofluids, *J. Therm. Anal. Calorim.* 143 (1) (2021) 767–779.
- [39] A. Bhattad, Experimental investigation of Al_2O_3 – MgO hot hybrid nanofluid in a plate heat exchanger, *Heat Transfer* 49 (4) (2020) 2344–2354.
- [40] A. Bhattad, J. Sarkar, Hydrothermal performance of plate heat exchanger with an alumina–graphene hybrid nanofluid: experimental study, *J. Braz. Soc. Mech. Sci. Eng.* 42 (2020) 1–10.
- [41] A. Bhattad, J. Sarkar, P. Ghosh, Heat transfer characteristics of plate heat exchanger using hybrid nanofluids: effect of nanoparticle mixture ratio, *Heat Mass Transf.* 56 (2020) 2457–2472.
- [42] A. Bhattad, Exergy analysis of plate heat exchanger with graphene alumina hybrid nanofluid: experimentation, *Int. J. Exergy* 33 (3) (2020) 254–262.
- [43] D.K. Mandal et al, Hybrid nanofluid magnetohydrodynamic mixed convection in a novel W-shaped porous system, *Int. J. Numer. Meth. Heat Fluid Flow* 33 (2) (2023) 510–544.
- [44] N. Biswas et al, Magneto-hydrothermal triple-convection in a W-shaped porous cavity containing oxytactic bacteria, *Sci. Rep.* 12 (1) (2022) 18053.
- [45] D.K. Mandal et al, Thermo-fluidic transport process in a novel M-shaped cavity packed with non-Darcian porous medium and hybrid nanofluid: Application of artificial neural network (ANN), *Phys. Fluids* 34 (3) (2022) 033608.
- [46] D.K. Mandal et al, Magneto-hydrothermal performance of hybrid nanofluid flow through a non-Darcian porous complex wavy enclosure, *Eur. Phys. J. Special Topics* 231 (13–14) (2022) 2695–2712.

- [47] M.K. Mondal et al, Positional impacts of partial wall translations on hybrid nanofluid flow in porous media: real coded genetic algorithm (RCGA), *Int. J. Mech. Sci.* 217 (2022) 107030.
- [48] N. Biswas et al, Enhanced energy and mass transport dynamics in a thermo-magneto-bioconvective porous system containing oxytactic bacteria and nanoparticles: cleaner energy application, *Energy* 263 (2023) 125775.
- [49] N.K. Manna et al, Impacts of heater-cooler position and Lorentz force on heat transfer and entropy generation of hybrid nanofluid convection in quarter-circular cavity, *Int. J. Numer. Meth. Heat Fluid Flow* 33 (3) (2023) 1249–1286.
- [50] N. Biswas et al, Implementation of partial magnetic fields to magneto-thermal convective systems operated using hybrid-nanoliquid and porous media, *Proc. Inst. Mech. Eng. C J. Mech. Eng. Sci.* 236 (10) (2022) 5687–5704.